Applied Catalysis B: Environmental 147 (2014) 988–999

Contents lists available at ScienceDirect

Applied Catalysis B: Environmental

journal homepage: www.elsevier.com/locate/apcatb

Are TiO_2-based exterior paints useful catalysts for gas-phase photooxidation processes? A case study on *n*-decane abatement for air detoxification

Ricardo A.R. Monteiro[a], Filipe V.S. Lopes[a], Adrián M.T. Silva[b,*], Joana Ângelo[c], Gabriela V. Silva[d], Adélio M. Mendes[c], Rui A.R. Boaventura[a], Vítor J.P. Vilar[a,*]

[a] *LSRE – Laboratory of Separation and Reaction Engineering, Associate Laboratory LSRE/LCM, Faculdade de Engenharia, Universidade do Porto, Rua Dr. Roberto Frias, 4200-465 Porto, Portugal*
[b] *LCM – Laboratory of Catalysis and Materials, Associate Laboratory LSRE/LCM, Faculdade de Engenharia, Universidade do Porto, Rua Dr. Roberto Frias, 4200-465 Porto, Portugal*
[c] *LEPAE – Laboratory for Process, Environmental and Energy Engineering, Faculdade de Engenharia, Universidade do Porto, Rua Dr. Roberto Frias, 4200-465 Porto, Portugal*
[d] *IDMEC – Institute of Mechanical Engineering, Faculdade de Engenharia, Universidade do Porto, Rua Dr. Roberto Frias, 4200-465 Porto, Portugal*

ARTICLE INFO

Article history:
Received 16 July 2013
Received in revised form
18 September 2013
Accepted 21 September 2013
Available online 29 September 2013

Keywords:
Photocatalysis
Air decontamination
n-Decane
Photo-TiO_2 paint
Acetate cellulose monoliths

ABSTRACT

n-Decane is a saturated long-chain hydrocarbon, belonging to the family of the volatile organic compounds (VOCs), which is persistently present in indoor air of several industrial closed facilities. Due to the VOCs environmental impact, all efforts that have been made during the last decades to degrade this kind of air pollutants are extremely important. Accordingly, the present paper reports *n*-decane photooxidation studies carried out in an annular photoreactor under simulated solar irradiation and employing a catalytic bed made of cellulose acetate monoliths coated with a photocatalytic paint. The influence of the feed flow rate, *n*-decane concentration, relative humidity, and incident irradiance on the *n*-decane degradation kinetics was assessed. Within this work, *n*-decane photodegradations higher than 90% were achieved, depending on the experimental conditions. Additionally, a phenomenological reaction rate model of the *n*-decane photocatalytic oxidation was proposed and assessed. The proposed model assumes that *n*-decane and water molecules compete for different active sites on the catalyst surface. Finally, despite the high *n*-decane photodegradation achieved, reaction by-products were identified and, based on these compounds, a reaction mechanism was formulated.

1. Introduction

For a long time, society has been debating indoor air pollution and its effect on human health whether in urban or industrial areas [1–4]. Today, 70–90% of our lifetime is spent at indoor environments [5,6]. Incoming air filters or air cleaners based on ultraviolet germicidal irradiation, activated carbon, ionization, or ozone generation are the most used methods for air decontamination [3,7]. Nevertheless, photocatalysis is now seen as a valuable option for de-polluting purposes [8–15], mainly because it: (i) can be operated at room temperature [16]; (ii) air (through water vapour and molecular oxygen) can be used as the source of oxidant [17]; (iii) degrades/mineralizes a wide range of organic pollutants into harmless or easily neutralized final products (CO_2, H_2O and mineral acids) [18]; (iv) can take advantage of solar radiation for performing the charge separation at the semiconductor [19]. Furthermore, semiconductor titanium dioxide (TiO_2) is commonly employed as photocatalyst in photocatalytic oxidation (PCO) processes due to its inexpensiveness, resistance to photocorrosion, high oxidative power, and relatively low toxicity [20–22].

As reported in our previous work [23], high concentrations of *n*-decane (up to 300 $\mu g\,m^{-3}$) were found in the indoor air of a WWTP with closed facilities at different sampling sites and campaigns; thus, *n*-decane was used as organic air pollutant model. The solar PCO of *n*-decane over TiO_2 for air detoxification can be represented by Eq. (1) [10]:

$$C_{10}H_{22}(g) + \frac{31}{2}O_2(g) \xrightarrow{TiO_2,h\upsilon} \text{intermediates} \xrightarrow{TiO_2,h\upsilon} 10CO_2(g) + 11H_2O(g) \quad (1)$$

* Corresponding authors. Tel.: +351 918257824; fax: +351 225081674.
E-mail addresses: adrian@fe.up.pt (A.M.T. Silva), vilar@fe.up.pt (V.J.P. Vilar).

0926-3373/$ – see front matter © 2013 Elsevier B.V. All rights reserved.
http://dx.doi.org/10.1016/j.apcatb.2013.09.031

and considering what is believed to be the initial stages of the photocatalytic process, the following equations are the most representative [24–27]:

$$TiO_2 + h\upsilon^+ \rightarrow e_{cb}{}^-(TiO_2) + h_{vb}{}^+(TiO_2) \quad (2)$$

$$h_{vb}{}^+(TiO_2) + H_2O \rightarrow HO + H^+ \quad (3)$$

$$h_{vb}{}^+(TiO_2) + H^- \rightarrow HO \quad (4)$$

$$e_{cb}{}^-(TiO_2) + O_2 \rightarrow O_2{}^- \quad (5)$$

$$HO + RH \rightarrow RH^+ \rightarrow R + H^+ \quad (6)$$

$$h_{vb}{}^+(TiO_2)\,RH \rightarrow RH^+ \rightarrow R + H^+ \quad (7)$$

$$O_2{}^- + H^+ \rightarrow HOO \quad (8)$$

$$O_2{}^- + HOO + H+ \rightarrow H_2O_2 + O_2 \quad (9)$$

Conduction-band electrons $e^-_{cb}(TiO_2)$ and valence-band holes $h^+_{vb}(TiO_2)$, i.e., electron–hole pairs, are generated when photons of energy $h\upsilon$ matching or exceeding the semiconductor band-gap energy are absorbed (Eq. (2)). Once at the surface of the semiconductor, and on the absence of any suitable acceptor (for e^-_{cb}) and donor (for h^+_{vb}) recombination will occur in a matter of nanoseconds; therefore no reaction occurs [16,27]. Hydroxyl anions and water molecules adsorbed on TiO_2 surface, act as electron donors, while molecular oxygen acts as electron acceptor, leading to the formation of hydroxyl (HO) and superoxide ($O_2{}^-$) radicals [24–26] (see Eqs. (3)–(5)). When an organic molecule (RH) is adsorbed onto semiconductor surface, the reaction with hydroxyl radical occur, followed by structural breakdown into several intermediates until, eventually, total mineralization (see Eq. (6)) [10,28]. The photogenerated holes due to the high oxidation potential can also participate in the direct oxidation of the organic pollutants (Eq. (7)) [29,30]. Peroxide (HOO) radical can also be generated from the protonation of $O_2{}^-$ radical and subsequently form hydrogen peroxide (see Eqs. (8) and (9)).

TiO_2 powders have been incorporated as white pigment in different applications from ancient times [31]. As early as 1929, Keidel [32] stated that titanium white pigment, under sunlight irradiation, was responsible for paint chalking because the photodegradation of organic binder. In 1938, Goodeve et al. [33] reported that UV absorption produces active oxygen species on the TiO_2 surface that cause dyes to photobleach.

Although, it was during the 1960s that, for the first time, TiO_2 photochemical effect was used to induce chemical reactions [34,35], Mashio and coworkers [36] in 1956 conducted several studies regarding oxidation induced by TiO_2 under illumination. These works concluded that anatase is more photoactive than rutile. However, the first contribution for understanding the heterogeneous photocatalytic effect was in 1972 with the pioneer work by Fujishima and Honda [37]. These authors investigated the electrochemical photolysis of water using a single TiO_2-rutile crystal (n-type) as photoanode and a Pt counter electrode. This work opened the frontiers for the use of titania for photocatalysis and other applications.

Construction materials can be used to support photocatalytic TiO_2 nanoparticles and used as depolluting agents [31,38–44]. Paint coatings, among all construction materials, are especially attractive as support for photocatalytic TiO_2 since almost all surfaces in urban areas can be painted. Bygott et al. [38], for instance, report a field trial in London, close to a school children playground, where an area of 300 m^2 of walls was painted with a silicate-based paint incorporating 7.5 wt.% of photocatalytic TiO_2. The results showed a daily NO_x abatement of ca. 4.5 g in about 10,000 m^3 of air around the school children playground [38]. Maggos et al. [44] report NO_x depollution tests in an artificially closed parking area, which was polluted by a car exhaust during the testing period; they observed a reduction of 19% and 20% for NO and NO_2, respectively. Salthammer and Fuhrmannh [43] studied the photocatalytic efficiency of two different types of commercially available wall paints in a 1 m^3 test chamber with and without air exchange using artificial daylight. The results showed that formaldehyde was photooxidise under static conditions. In contrast, for typical VOCs, under dynamic conditions, no significant photocatalytic effect was observed.

Several studies indicate that paint components can impair the photoactivity of paint films [42–50]. For example, Allen et al. [46] studied the effect of different paint components on the photoactivity of these paints. The results showed that the porosity, which is related to the particulated paint components (pigments and extenders) concentration, has a positive effect on photoactivity. However, higher content in $CaCO_3$ and high porosity makes paints prone to self-degradation. In the same line, Águia et al. [41,51,52] developed a vinyl exterior paint modified with several TiO_2 photocatalysts: P25 (Evonik/Degussa), PC50 (Millennium), PC105 (Millennium), PC500 (Millennium), ANX type PA (Kemira), UV100 (Sachtleben), AMT100 (Tayca), UVLP7500 (Kronos), VLP7000 (Kronos), and VLP7101 (Kronos); the authors stated that paint pigmentary TiO_2 is the most critical component affecting the photocatalytic activity for NO_x abatement due to its competitive absorption of the UV radiation. Considering the results reported by these authors, the highest yields towards NO_x photocatalytic oxidation are obtained when incorporating in paint formulations photocatalysts PC500 (Millennium), PC105 (Millennium), and UV100 (Sachtleben) [41,51,52].

Although the potential of photocatalytic paints to detoxify air is very promising, several studies demonstrate the formation of by-products that may be harmful for humans [45,53–55]. For example, Uhde and Salthammer [54] reported that UV-irradiated paints produce undesired and highly toxic by-products such as formaldehyde, acetaldehyde, ethylacrolein, pentanal, 1-hydroxy-butanone, and hexanal. This observation was further emphasized by Kolarik and Toftum [53]. Auvinen et al. [45] and Geiss et al. [55] found that relatively high amounts of organic compounds, such as aldehydes and ketones, are formed from the decomposition of binders and additives. Auvinen et al. [45] also stated that photocatalytic surface ageing and the use of different substrates (glass, gypsum or polymeric plaster) do not have a noteworthy influence on the paint photocatalytic activity.

Disinfection of air using photocatalytic paints was the focus of other research groups [47,50,56]. According to Hochmannova and Vytrasova [47], UV light emitted from normal domestic fluorescent lights is capable to ensure the photocatalytic and antimicrobial effects of paints incorporating nanoparticles of zinc oxide. Later, Sousa et al. [50] showed microorganism photoinactivation over a photocatalytic paint under UVA irradiation.

Although photocatalytic paints have been showing very promising results concerning the photodegradation of air pollutants and the photoinactivation of microorganisms, it is necessary to keep improving their performance paints as well as understand the phenomena behind their photoactivity. This paper presents a study on gas-phase solar photooxidation of *n*-decane over a TiO_2-containing paint, using a lab-scale continuous-flow annular photoreactor with a compound parabolic collector. To the best of our knowledge, this is the first time that the performance of TiO_2-based exterior paints and their applicability on gas-phase photooxidation processes for *n*-decane abatement is evaluated. The photocatalytic oxidation of *n*-decane was studied for different operating conditions, such as feed flow rate, *n*-decane

Table 1
Catalyst and paint properties; catalytic bed characteristics; photoreactor dimensions employed in the gas-phase PCO of *n*-decane under simulated solar irradiation.

Catalyst and paint [51,52]		
PC500	Manufacturer	PC500 (Millennium)
	Crystal structure	>99% Anatase
	Crystal size (nm)	5–10
	Shape	Agglomerates
	Surface area ($m^2\ g^{-1}$)	345
	Agglomerate size (μm)	1.2–1.7
Exterior water-based vinyl paint	Shape	Agglomerates
	Pigmentary TiO_2	18 wt.% (wet basis)
	Water	30 wt.% (wet basis)
	Extenders ($CaCO_3$ and silicates)	18 wt.% (wet basis)
	Polymer extender slurry	8 wt.% (wet basis)
	Binder slurry	20 wt.% (wet basis)
	Additives (in slurry)	6 wt.% (wet basis)
Catalytic bed (PC)		
Catalyst (P)	TiO_2 content (wet basis)	
	Pigmentary	9 wt.% (wet basis)
	PC500	9 wt.% (wet basis)
Support (C)	Thin-film properties	
	m_P (g)	1.052
	ρ_P ($g\ cm^{-3}$)	2.61
	mc_C (g)	2.006
	ρ_C ($g\ cm^{-3}$)	1.30
	d_{ch} (cm)	0.9
Porosity	ε	0.991
Photoreactor		
Outer tube (Pyrex-glass)	$d_{ot,e}$ (cm)	5.00
	$d_{ot,i}$ (cm)	4.64
Inner tube (quartz)	$d_{in,e}$ (cm)	2.00
	$d_{in,i}$ (cm)	1.64
Photoreactor	L_R (cm)	16.0
	V_R (cm^2)	220

concentration, feed relative humidity and incident irradiance. The *n*-decane degradation reaction behaviour in the continuous system was modelled considering different Langmuir-Hinshelwood kinetic-based reaction rate equations. It considers that PCO of *n*-decane is not influenced by reaction intermediates and/or products and *n*-decane and water are the major species. In addition, a reaction mechanism was proposed for *n*-decane PCO considering the degradation by-products identified by GC/MSD.

2. Experimental

2.1. Materials and chemicals

Mendes et al. [41,51,52] reported a water-based vinyl paint loaded with TiO_2 photocatalyst PC500 (Millennium) that produced high NO conversions among several other commercially available photocatalysts. For this reason the same modified vinyl paint with photo-TiO_2 PC500 was selected. The PC500 photocatalyst properties are detailed in Table 1. Cellulose acetate monoliths (named C:TIMax CA50-9/$S - L_C$ = 80 mm, $d_{ch}^2 = 9\ mm \times 9\ mm$, $e_{w,ch}$ = 0.1 mm; Wacotech GmbH & Co. K.G.) were used to support the catalytic paint. For the generation of humidified air streams contaminated with *n*-decane, deionized water and *n*-decane (≥94%; CAS no. 124-18-5; Merck) were used without further purification. Air Liquide provided all gases, with minimum total purities of 99.999%: helium N50, nitrogen N50, and synthetic air N50 (O_2: 20 ± 1%; H_2O: <3 ppm; C_nH_m: <0.1 ppm; CO_2: <1 ppm; CO: <1 ppm).

2.2. Photocatalytic films preparation and characterization

Photo-TiO_2 PC500 from Millennium was used to modify a commercially available exterior water-based vinyl paint. The catalyst and paint properties are summarized in Table 1 [52]. From the original exterior water-based vinyl paint, half of the pigmentary TiO_2 (9 wt.% in wet base) was removed; the photocatalytic paint (henceforth named as P) was, subsequently, formulated by adding 9 wt.% of photo-TiO_2 PC500 (ca. 50 cm^3 of paint without 50% of pigmentary TiO_2 and mixing for 30 min at 300 rpm in a 100 cm^3 stainless steel vessel), as reported by Águia et al. [41]. The final photo-TiO_2 PC500 and pigmentary TiO_2 content was 9 wt.% in wet basis (ca. 17 wt.% in dry basis) (see Table 1).

Cellulose acetate monoliths were coated with a thin film of the photocatalytic paint P using the dip-coating method (Dip-Coater RDC21-K, Bungard Elektronik GmbH & Co. K.G.) [57]; the photocatalytic paint supported on cellulose acetate monoliths was labelled as PC. Briefly, before coating, cellulose acetate samples were soaked for 1 h with distilled water and alkaline detergent (Derquim LM 01, Panreac Química, S.A.U.), subsequently washed exhaustively with Milli-Q water, and finally, heated up to 323 K to dryness. Then, four layers of photocatalytic paint P were deposited at a withdrawal rate of 0.8 $mm\ s^{-1}$ until a thin and uniform film was formed on each support surface (these samples were dried at 323 K for 1 h between each layer deposition). Finally, PC samples were packed into an annular photocatalytic reactor (see Section 2.4) for the study of *n*-decane degradation through PCO. The catalytic bed properties are also detailed in Table 1.

Scanning electron microscopy (SEM) coupled with energy dispersive X-ray (EDX) analysis was performed in a FEI Quanta 400 FEG ESEM/EDAX Genesis X4M apparatus equipped with a Schottky field emission gun (for optimal spatial resolution) for the characterization of the surface morphology of PC500 powder, fresh PC, and used PC samples (after more than 50 h of PCO experiments) as well as their chemical composition. Each sample was mounted on a double-sided adhesive tape made of carbon for its surface observation at different magnifications; the cross-section of the fresh PC sample was also measured by this technique. These SEM/EDX analyses were made at CEMUP (Centro de Materiais da Universidade do Porto).

2.3. Experimental setup

The experimental setup is depicted in Fig. 1. A full description of the whole apparatus is given elsewhere [58]. The feed generator is composed by three mass flow controllers (MFC, El-Flow, Bronkhorst High-Tech B.V.), which allow the generation of humid air streams contaminated with *n*-decane by flowing air through distinct Woulff bottles (Normax, Lda.), one containing *n*-decane and another filled with deionized water (Fig. 1a). The photocatalytic system comprises (Fig. 1b): (i) a solar simulator (Atlas, model Suntest XLS+) with a working area of 0.110 m^2, a 1.7 kW air-cooled xenon arc lamp, a daylight filter and quartz filter with infrared coating; (ii) a compound parabolic collector with 0.023 m^2 of illuminated area with electropolished anodized aluminium reflectors (to use both direct and diffuse irradiation as well to uniform it throughout the bed); (iii) photoreactor composed by two concentric and axially centred tubes (the outer tube made of Pyrex-glass, Duran borosilicate glass 3.3, cut-off at 280 nm, Schott-Rorhglas GmbH, and the inner tube made of quartz, Quarzglas-Rohr Quarzglastechnik, GmbH & Co.); (iv) an actinic lamp (Actinic BL TL 6W, Koninklijke Philips Electronics N.V.) for catalyst degassing and activation purposes, placed inside and axially centred in the inner tube (peak at 365 nm – UVA radiation). Both inlet and outlet caps of the photoreactor have four equidistant inlets to ensure a better distribution of the feed stream to the reactor. Note that the tubing for inlets and outlets are made of PTFE (supplied by Vidrolab2, S.A.) that minimizes the adsorption of VOCs. Table 1 also shows the tube dimensions of the photoreactor; Fig. 1b_1 and b_2 schematically represent the continuous-flow photoreactor from a side and frontal point of view, respectively.*n*-Decane concentration

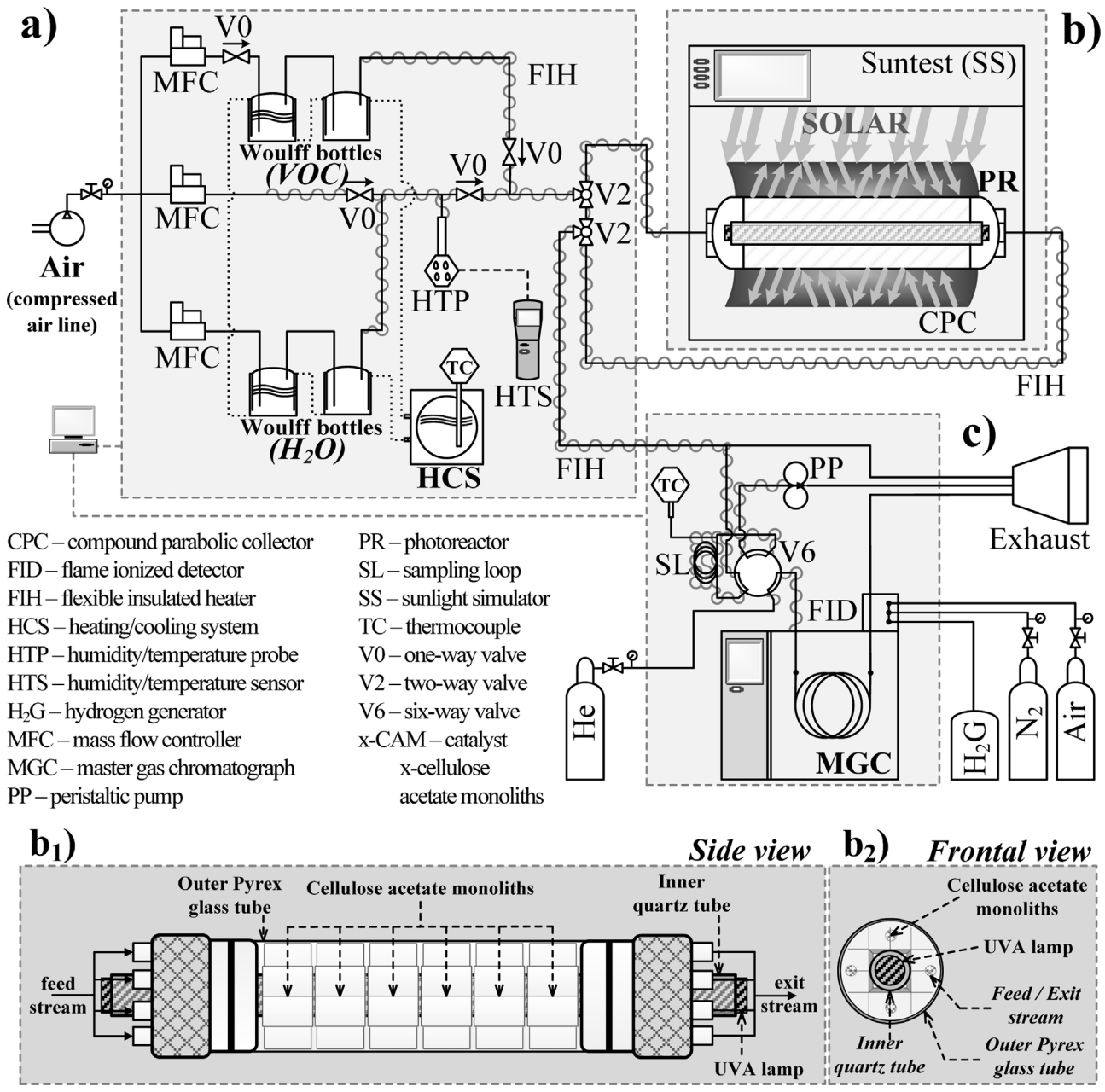

Fig. 1. Schematic representation of the experimental set-up and the continuous-flow photoreactor: (a) lab-scale unit used for the generation of air streams containing *n*-decane and water vapour; (b) sunlight simulator containing the photoreactor: (b_1) from a side point of view and (b_2) from a frontal point of view; (c) master gas chromatograph analytic system used for the analysis of the photoreactor feed and exit streams.

Source: Reprinted (adapted) with permission from Lopes et al. [58]. Copyright© 2012, Elsevier.

histories were monitored using a gas chromatograph (MGC Fast GC, Dani Instruments S.p.A.) equipped with a flame ionization detector (FID) and a Volcol capillary column (20 m × 0.18 mm × 1.00 μm; Supelco, Sigma–Aldrich Co. LLC) (see Fig. 1c). The experimental setup was connected to a computer and controlled using a data acquisition board system and an in-house programme developed routine written in Labview environment (NI Corporation). All connections are of 1/16 in. stainless steel tubing (Swagelok Company) to reduce dead volumes.

Additionally, by-products from the *n*-decane photooxidation were analyzed at steady-state, sampling the photoreactor exit stream to a Tedlar bag (232-05SKC, SKC Inc.) and then transferring the sample to stainless steel tubes with Tenax TA60/80 mesh (Supelco, Sigma–Aldrich Co. LLC.). After sampling, identification and quantification of the reaction products was performed with a thermal desorption system (SDT 33.50, Dani Instruments S.p.A.) working in line with a GC/MSD device (a gas chromatograph GC 6890N coupled to a mass spectrometer detector MSD 5973, Agilent Technologies, Inc.). The response factor of toluene (ISO 16000-6 [59]) was used to determine the concentration of the major products (while for *n*-decane, specific response factor were used).

2.4. Photocatalytic experiments

All experiments were carried inside the chamber of the aforementioned solar simulator, which can simulate a spectrum similar to that of sunlight within $300 < \lambda < 800$ nm. The incident irradiance was measured using a broadband UV radiometer (CUV 5, Kipp & Zonen B.V.), placed on the outside of the outer tube and at the same

Table 2
Experimental conditions employed in the study of *n*-decane photodegradation.

Run	Q_{feed} [a] ($cm^3\ min^{-1}$)	$C_{dec,\ feed}$ (ppm)	RH_{feed} [a] (%)	I [b] ($W\ m^{-2}$)
1[c]	150	73	40	38.4
2	150	73	40	29.1
3	150	73	40	18.9
4	75	73	40	38.4
5	75	73	40	29.1
6	75	73	40	18.9
7	300	73	40	38.4
8	300	73	40	29.1
9	300	73	40	18.9
10	150	40	40	38.4
11	150	40	40	29.1
12	150	40	40	18.9
13	150	138	40	38.4
14	150	138	40	29.1
15	150	138	40	18.9
16	150	73	3	38.4
17	150	73	3	29.1
18	150	73	3	18.9

[a] Measured at 298 K and 1 bar.
[b] Measured within 280–400 nm (sunlight UV fraction).
[c] Operating conditions used for photochemical experiment.

height, within a spectral range of 280–400 nm corresponding to the UV fraction of the solar irradiation.

At steady-state, *n*-decane photodegradation fraction ($C_{dec,\ exit}/C_{dec,\ feed}$, where $C_{dec,\ feed}$ and $C_{dec,\ exit}$ in ppm are the pollutant concentration on the feed and exit streams, respectively) was studied for several experimental conditions: feed flow rate (75–300 $cm^3\ min^{-1}$, measured at 1 bar and 298 K), pollutant concentration (40–138 ppm), feed relative humidity (3–40%, measured at 1 bar and 298 K), and incident irradiance (18.9–38.4 $W\ m^{-2}$, measured for the spectral range between 280 and 400 nm: UV fraction of the incident sunlight). Table 2 summarizes all the experiment conditions. Prior to all experiments, the catalytic bed was degassed and the photocatalytic paint coat activated under UV radiation and by flowing 30 mL min^{-1} (measured at 1 bar and 298 K) of synthetic air with 40% of relative humidity for 24 h (similar conditions as described elsewhere [41]). Before turning on the solar simulator, the catalytic bed was continuously fed and, by means of outlet stream sampling analysis, the feed composition steadiness was checked.

3. Results and discussion

3.1. Photochemical oxidation of n-decane

A blank test consisting in an experiment without photocatalyst was performed, showing no measurable *n*-decane concentration decrease (data not presented; operating conditions reported in Table 2: run 1).

3.2. Photocatalytic oxidation of n-decane

3.2.1. Surface characterization of photo-TiO_2 powder and PC samples

The surface morphology of PC500 powder sample and its chemical composition were determined by SEM/EDX. The SEM micrograph (Supplementary Data: Fig. A.1) shows an estimated size of the photo-TiO_2 agglomerates of ca. 600–1500 nm. According to this image, the dimension of the agglomerates range from half size up to the values provided by the manufacturer (see Table 1); similar sizes are displayed in SEM pictures of photocatalytic paint films loaded with the same photocatalyst and reported by Aguia et al. [51]. As previously mentioned by the same authors [51], EDX analysis of PC500 powder (Supplementary Data: Fig. A.2) indicates that both agglomerates and individual particles are only made of TiO_2.

The surface morphology and chemical composition of PC samples was also determined by SEM/EDX. SEM micrographs of fresh PC and used PC samples (with 50 h+ of use in PCO of *n*-decane) at three different magnifications are shown in Fig. 2a–d. The fresh PC images (Fig. 2a and c) show that the photocatalytic paint was homogeneously coated on the cellulose acetate monolith. After its use on the PCO experiments (Fig. 2b and d), SEM micrographs suggest that the film structure was not significantly affected despite the harsh operating conditions employed. This conclusion was also supported by EDX analysis of both fresh and used samples (shown in Fig. 2e and f, respectively). According to the EDX spectra, the proportion of each element remained approximately the same after the photocatalytic experiments. From SEM images (Fig. 3) it was also possible to estimate the paint film thickness (ca. 5–10 μm) and the cellulose acetate monolith thickness (ca. 50 μm). Contrarily to what have been observed by Lopes et al. [60] when using TiO_2 sol–gel films supported on cellulose acetate monoliths, paint films are approximately 25-fold thicker (and more resistant) than TiO_2 sol–gel films. These properties significantly prevent film fissures, delamination, and/or degradation. Thus, the use of paint films reveals to be an advantage in the prevention of the catalyst/support ageing.

3.2.2. Operating parameters effect on n-decane photodegradation

At steady-state conditions, *n*-decane photodegradation fraction ($C_{dec,\ exit}/C_{dec,\ feed}$) was obtained for four experimental conditions (Figs. 4–6). Fig. 4 shows the effect of the feed flow rate (Q_{feed}) on the *n*-decane photodegradation fraction. *n*-Decane photodegradation decreases as Q_{feed} increases, since a higher feed flow rate results in a lower residence time, reducing the pollutant-catalyst contact period. Thereby, for a 4-fold increase in Q_{feed}, the photocatalytic process is 1.6, 1.9, and 2.3 times less effective, respectively, for incident irradiances of 38.4, 29.1 and 18.9 $W\ m^{-2}$ (Table 2: runs 4 and 7, runs 5 and 8, and runs 6 and 9, respectively). This also means that, for a higher feed flow rate the incident irradiance on the catalyst surface becomes more relevant for the PCO of *n*-decane: the electron–hole pairs formation is favoured by higher incident irradiances.

Fig. 5 shows the influence of the feed concentration on the *n*-decane photodegradation fraction. Results show a decrease in the photodegradation fraction with an increase of *n*-decane concentration. In fact, for a 3.4-fold increase in *n*-decane concentration, 1.8, 2.4, and 3.6 times lower photodegradation fractions were observed for incident irradiances of 38.4, 29.1 and 18.9 $W\ m^{-2}$, respectively (Table 2: runs 4 and 7, runs 5 and 8, and runs 6 and 9, respectively). So, increasing the number of *n*-decane molecules that enters the reactor per unit of time, a higher number of photons/hydroxyl radicals are necessary to achieve the same photodegradation. Furthermore, the results above suggest that the feed concentration has a more important influence on the PCO of *n*-decane than the feed flow rate for the same organic load, most likely due to the considerably lower surface area "usefully" available for the photocatalytic reaction. In other words, despite the equivalent UV-irradiated surface area, there are more VOC molecules adsorbed per surface area, restricting the generation of oxidant species from adsorbed water and oxygen (namely, hydroxyl radicals, peroxide radicals, and superoxide radicals).

Although there are plenty of studies describing the influence of feed relative humidity on the photodegradation of alkanes, conclusions are still not clear [10,61]. Twesme et al. [62] and Zhang and Liu [63] pointed out 40% and 20% of relative humidity, respectively, as the optimum conditions regarding water content to obtain the highest degradation rates in their studies. Shang et al. [64] demonstrated in their studies that the degradation rate of *n*-heptane

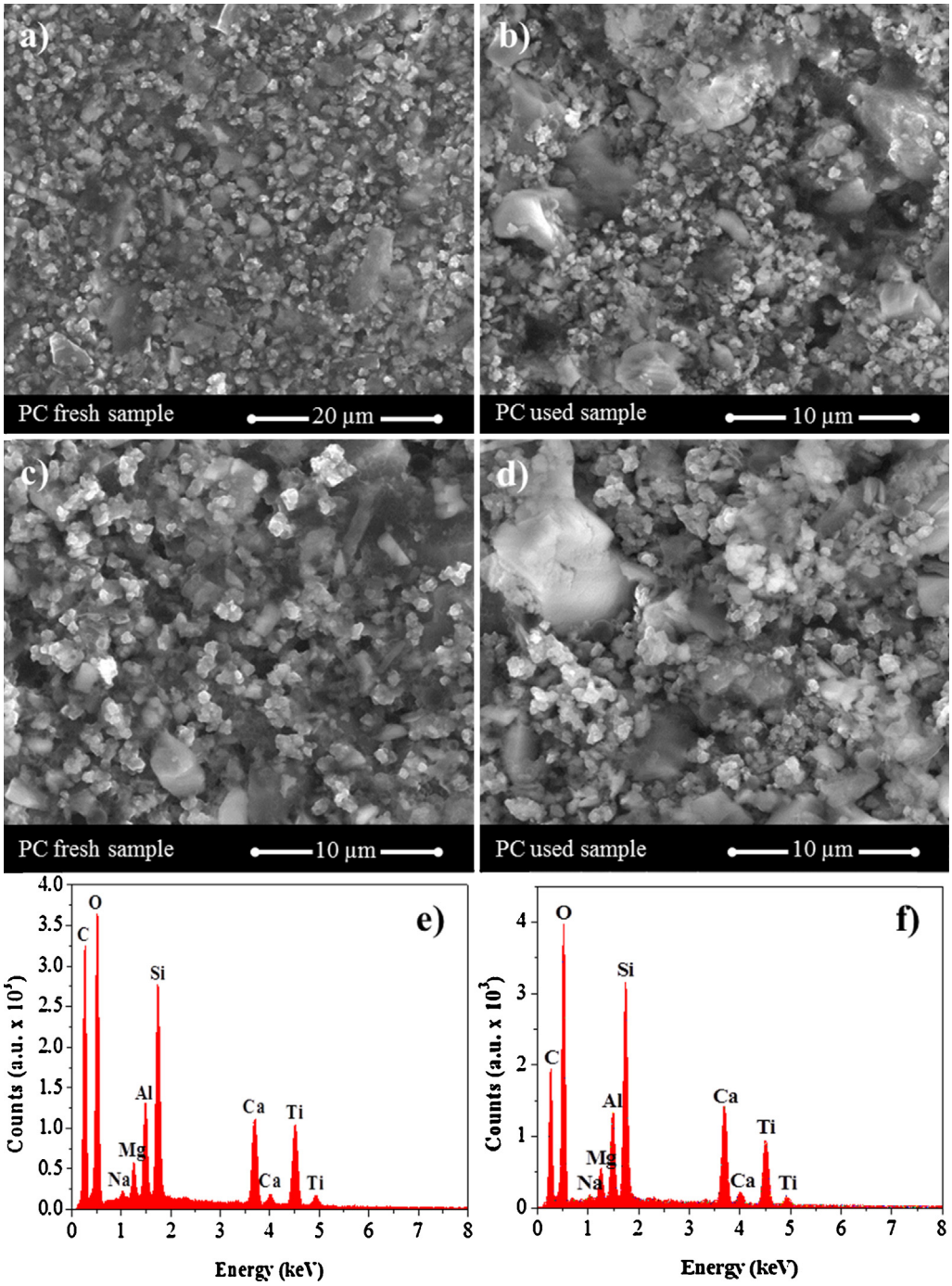

Fig. 2. SEM micrographs (a–d) and EDX spectra (e and f) of PC before (left-side images) and after 50 h+ of use (right-side images) in PCO of *n*-decane.

decreases as the relative humidity was increased from 0 to 60%. In fact, the presence of vapour water molecules has two opposing effects: (i) inhibits the degradation by competitive adsorption to the photocatalyst surface (for feed streams with high water vapour content) [6,65]; (ii) accelerates the degradation by promoting hydroxyl radicals formation [25]. Fig. 6 shows a slight relative increase (3%) of the *n*-decane photodegradation for the highest irradiance value (38.4 W m^{-2}) and within the relative humidity range of 3–40%. On the other hand, it was found that for the lower irradiance values, particularly for 18.9 W m^{-2}, its effect on the *n*-decane photodegradation becomes more relevant: for the same relative humidity increment, the *n*-decane photodegradation is 3% (from run 16 to run 1) to 25% (from run 18 to run 3) more efficient with a 2-fold reduction of the incident irradiation (from 38.4 to 18.9 W m^{-2}). This supports the important role of hydroxyl radicals in photocatalytic processes due to the lower amount of surface electron–hole pairs available on the catalyst surface to react with the pollutant molecules.

It should be pointed out that after 50 h under simulated solar irradiation and continuous feed (humid air contaminated with *n*-decane), similar photodegradations were obtained under the same operating conditions (data not shown). Considering the up-stated for SEM analysis (see Section 3.2.1), it is suggested that PC deterioration was negligible.

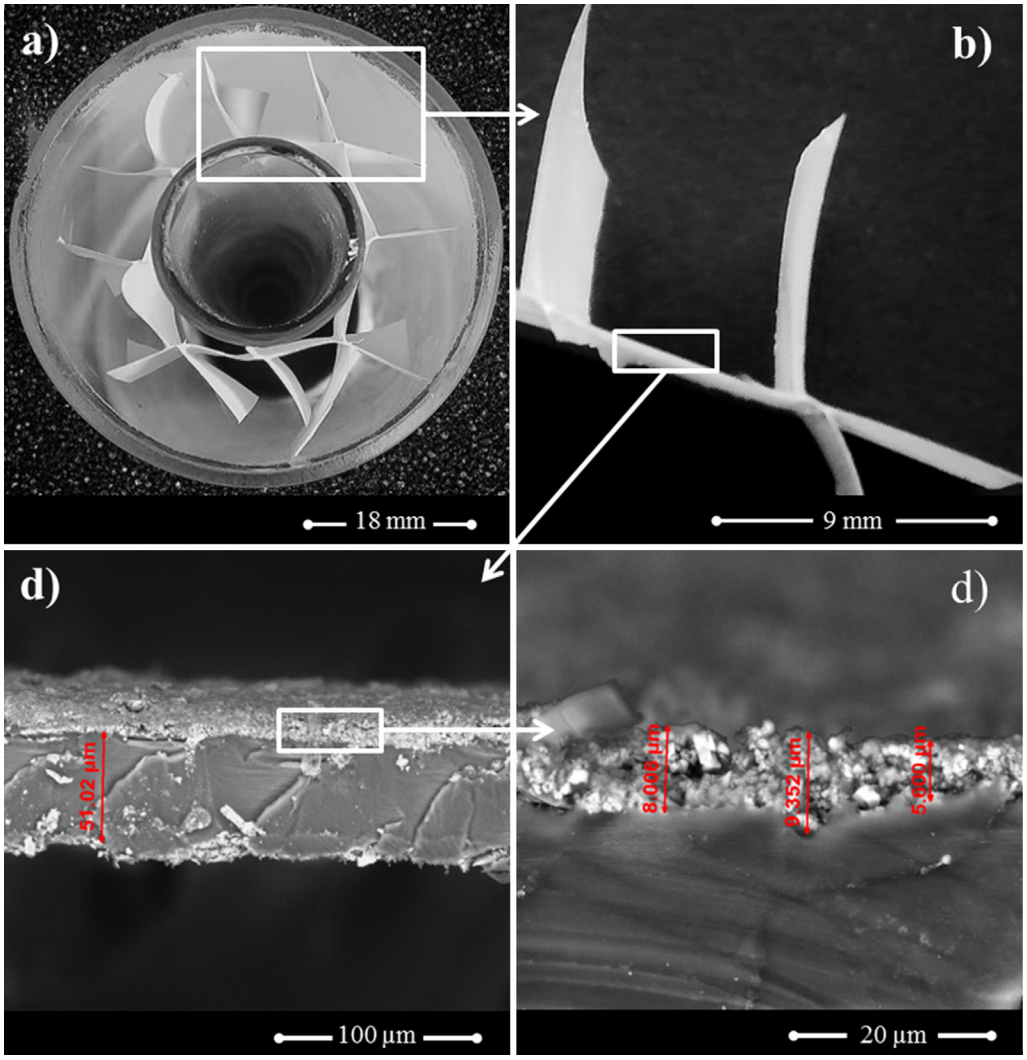

Fig. 3. Photographs (a and b) and SEM micrographs (c and d) of PC after 50 h+ of use in PCO of *n*-decane.

3.2.3. Simulation and predictive studies of n-decane kinetics through PCO

Several models have been proposed in the literature for simulating VOC photocatalytic oxidation kinetics [58,60]. Table 3 describes the complete mathematical model combined with three different Langmuir-Hinshelwood reactions rate expressions. The numerical solution of the mathematical model was performed in gPROMS environment (Process System Enterprise, London, UK) using the orthogonal collocation on finite elements method. The number of elements used was 90 with two interior collocation points (third order polynomials) in each element of the photocatalytic bed. The simulations were performed with an absolute and relative tolerance of 1×10^{-5}. First, parameters were estimated using a sequential quadratic programming algorithm [60]; then, the mathematical model was employed for simulating the PCO of *n*-decane. Table 3 reports the estimated kinetic and adsorption equilibrium parameters.

Results shows that the mathematical model with the Langmuir-Hinshelwood kinetic reaction rate expression RE-3 (bimolecular competitive two types of sites rate expression) generally produced better fitting results within the operational conditions studied than models RE-1 or RE-2 (bimolecular competitive one type of sites or bimolecular non-competitive two types of sites rate expressions) (Figs. 4–6). This means that both *n*-decane and water molecules must be considered independent and targeting different active sites of the catalyst surface. The surface active sites competition between the two types of molecules cannot be disregarded because, despite the higher number of parameters required by RE-3, this rate expression is more suitable to describe the experimental data (see the statistical analysis reported in Table 3). Contrarily to the previous reported models of PCO [58,60], it was necessary to include an incident irradiance exponential order constant (n). The radial effect of the UV irradiation passing through the PC samples and its consequent reflection and refraction were not considered; moreover, the mathematical model neglects any partial UV absorption by the PC samples. Nevertheless, the UV irradiance on PCO of *n*-decane could be fitted by an irradiance exponential order constant $n = 0.8$, as can be seen throughout the paper (Figs. 4–6).

The closest results to our data regarding gas-phase PCO of *n*-decane were obtained by Debono et al. [66]. However, these authors performed UVA-photocatalytic experiments of *n*-decane over TiO_2 powder dispersed at the bottom of a batch reactor, and employing *n*-decane-polluted air stream at ppb level. Therefore and only for these conditions Debono et al. [66] were able to provide a photocatalytic lab-scale setup effective for complete *n*-decane photodegradation.

Considering that the mathematical model described successfully the reported experiments, simulations can now be performed to obtain insights concerning the effect of each operating variable on the process performance. The effect of the lab-unit geometrical

Table 3
Mathematical model, boundary conditions, kinetic reaction rate expressions used for estimation of the kinetic and adsorption equilibrium parameters of the PCO of *n*-decane; estimated kinetic and adsorption equilibrium parameters resulting of the mathematical model.

Mathematical model, correlations, parameters, and boundary conditions [58,60]

Material balance for each component *i*	$\frac{d}{dz}\left(\varepsilon D_{ax}\frac{dC_i}{dz}\right) - \frac{d}{dz}(\tilde{u}_{0,ch}C_i) - \nu_i \quad r = 0$
Axial dispersion (laminar flow) [81–84]	$D_{ax} = D_m + (1/192)[(\tilde{u}_{0,ch}^2 d_{ch}^2)/(\varepsilon D_m)]$
Molecular diffusivity of the mixture	$D_m \cong \frac{1}{N}\sum_{i=1}^{N} D_{m,i}$, with $D_{m,i} = (1-y_i)\sum_{\substack{i=1 \\ j\neq i}}^{n} D_{ij}/y_i$
Binary diffusion coefficient [85–88]	$D_{ij} = \frac{1.41\times10^{-7}T^{1.75}[1/2(M_i^{-1}+M_j^{-1})]^{1/2}}{p[(\Sigma_v)_i^{1/2}+(\Sigma_v)_j^{1/3}]^2}$
Superficial velocity (in the cross-section of each channel)	$\tilde{u}_{0,ch} = Q_{feed}[\pi(1/2(d_{ot,i}))^2 - \pi(1/2(d_{in,e}))^2]^{-1}$

Component *i*	N_2	O_2	H_2O	dec
M_i (g mol^{-1})	28.01	32.00	18.02	142.28
$(\Sigma_v)_i$	18.5	16.3	13.1	209.8
Boundary conditions	Photoreactor feed ($z=0$)		Photoreactor exit ($z=L_R$)	
	$u_{0,feed}C_{i,feed} = \tilde{u}_{0,ch}C_i - \varepsilon D_{ax}\frac{dC_i}{dz}\Big\vert_{z=0}$		$\frac{dC_i}{dz}\Big\vert_{z=L_R} = 0$	

Kinetic reaction rate expressions [3,6,58,60,89–95]

RE-1	$r_{dec} = I^n \cdot k\left(\frac{K_{dec}K_{H_2O}C_{dec}C_{H_2O}}{(1+K_{dec}K_{H_2O}C_{dec}C_{H_2O})^2}\right)$	*Langmuir-Hinshelwood bimolecular competitive one type of sites*
RE-2	$r_{dec} = I^n \cdot k\left(\frac{K_{dec}C_{dec}}{1+K_{dec}C_{dec}}\right)\left(\frac{K_{H_2O}C_{H_2O}}{1+K_{H_2O}C_{H_2O}}\right)$	*Langmuir-Hinshelwood bimolecular non-competitive two types of sites*
RE-3	$r_{dec} = I^n \cdot k\left(\frac{K_{dec}C_{dec}}{1+K_{dec}C_{dec}+K_{H_2O}C_{H_2O}}\right)\left(\frac{K'_{H_2O}C_{H_2O}}{1+K'_{dec}C_{dec}+K'_{H_2O}C_{H_2O}}\right)$	*Langmuir-Hinshelwood bimolecular competitive two types of sites*

Kinetic reaction and rate expressions	RE-1	RE-2	RE-3
Estimated parameters			
Kinetic and adsorption equilibrium parameters			
n	0.8	0.8	0.8
k (mol m^{-2} s^{-1} (W^{-1} m^2)^n)	1.0×10^{-5}	3.2×10^{-6}	2.8×10^{-6}
K_{dec} (M^{-1})	13	2205	4498
K_{H_2O} (M^{-1})	9.7×10^{-5}	1.5×10^{-4}	1.0×10^{-8}
K'_{dec} (M^{-1})	–	–	905
K'_{H_2O} (M^{-1})	–	–	4.6×10^{-4}
Statistics			
R^2	0.764	0.912	0.954
S_R^2 ($\times10^7$ mol^2 m^{-4} s^{-2})	3.84	1.43	0.874

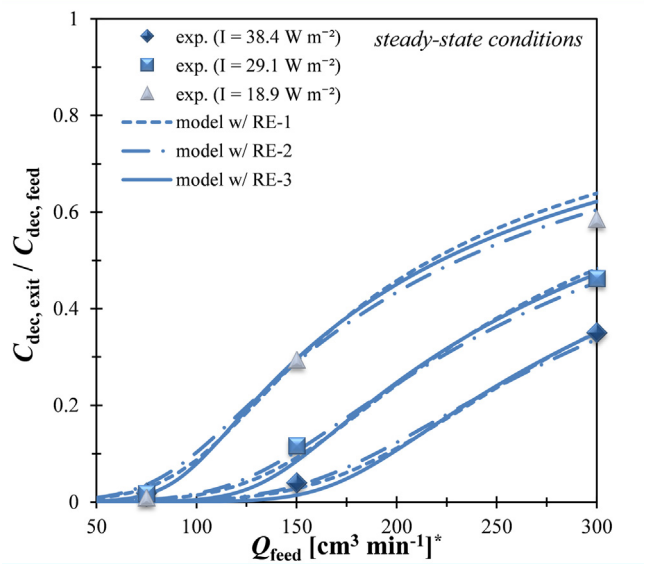

Fig. 4. Influence of feed flow rate (Q_{feed}) on *n*-decane photodegradation fraction ($C_{dec,exit}/C_{dec,feed}$, at steady-state conditions): experimental points for incident irradiances measured within 280–400 nm (sunlight UV fraction) of 38.4 W m^{-2} (◆), 29.1 W m^{-2} (■), and 18.9 W·m^{-2} (▲), and RE-1 (– – –), RE-2 (– • –), and RE-3 (———); $C^*_{dec,feed} = 73$ ppm, $RH^a_{feed} = 40\%$, and $T = 298$ K; operation conditions reported in Table 1; * Measured at 298 K and 1 bar.

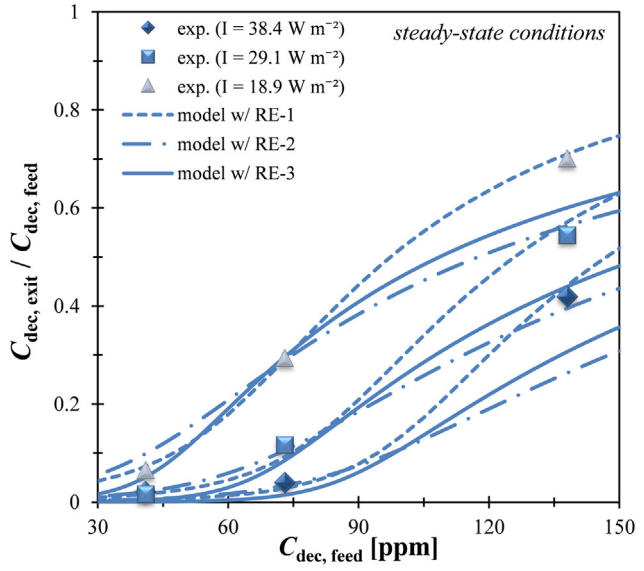

Fig. 5. Influence of the inlet concentration ($C_{dec,feed}$) on *n*-decane photodegradation fraction ($C_{dec,exit}/C_{dec,feed}$, at steady-state conditions): experimental points for incident irradiances measured within 280–400 nm (sunlight UV fraction) of 38.4 W m^{-2} (◆), 29.1 W m^{-2} (■), and 18.9 W m^{-2} (▲), and RE-1 (– – –), RE-2 (– • –), and RE-3 (———); $Q^*_{feed} = 150$ cm^3 min^{-1}, $RH^a_{feed} = 40\%$, and $T = 298$ K; operation conditions reported in Table 2; * Measured at 298 K and 1 bar.

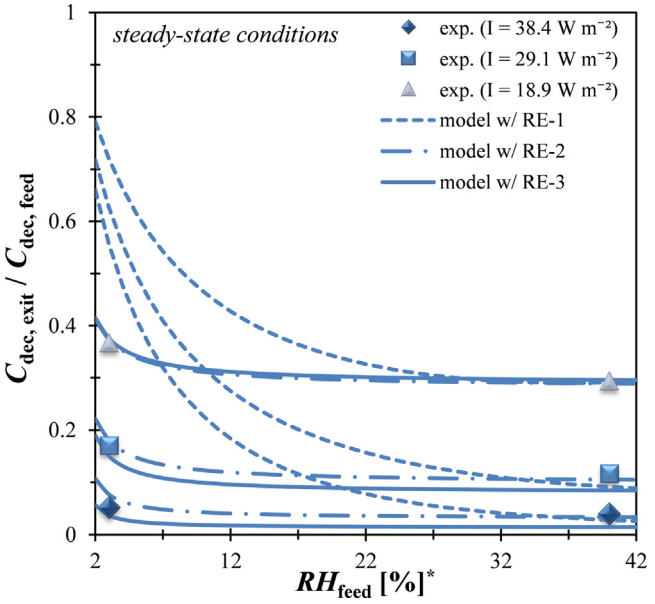

Fig. 6. Influence of the feed relative humidity (RH_{feed}) on *n*-decane photodegradation fraction ($C_{dec,\,exit}/C_{dec,\,feed}$, at steady-state conditions): experimental points for incident irradiances measured within 280–400 nm (sunlight UV fraction) of 38.4 (◆), 29.1 (■), and 18.9 W m^{-2} (▲), and RE-1 (– – –), RE-2 (– • –), and RE-3 (———); Q^{*}_{feed} = 150 cm^3 min^{-1}, $C_{dec,\,feed}$ = 73 ppm, and T = 298 K; operation conditions reported in Table 2; * Measured at 298 K and 1 bar.

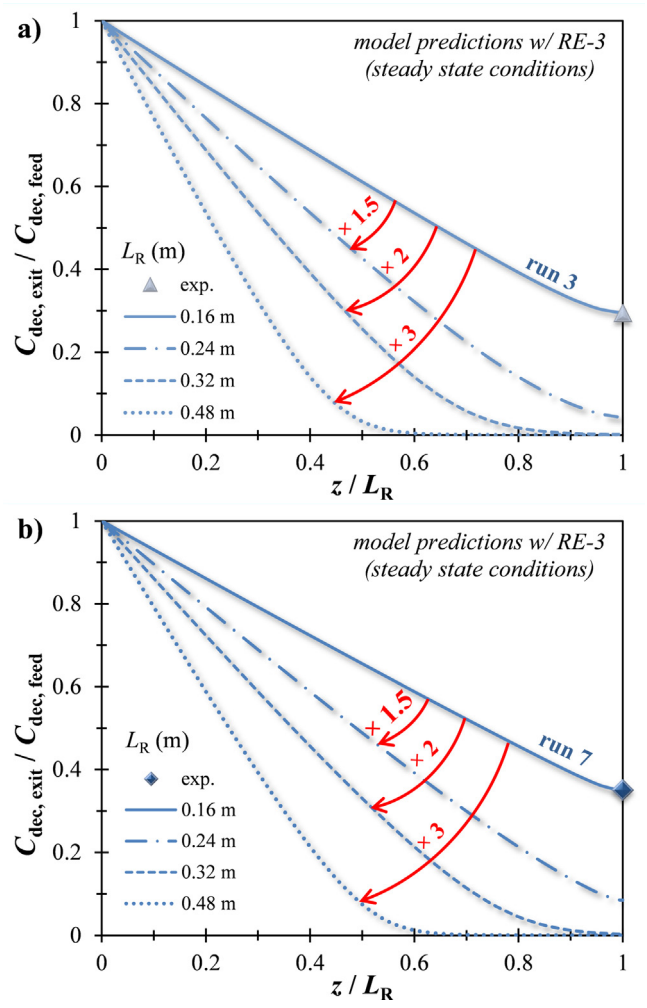

Fig. 7. *n*-Decane photodegradation fraction profiles ($C_{dec,\,exit}/C_{dec,\,feed}$, at steady-state conditions) for photoreactors with different lengths [L_R]: 0.16 (———), 0.24 (— — —), 0.32 (- - -), and 0.48 m (• • •); (a) $C_{dec,\,feed}$ = 73 ppm, Q^{*}_{feed} = 150 mL min^{-1}, and I = 18.9 W m^{-2} (measured within 280–400 nm: sunlight UV fraction); (b) $C_{dec,\,feed}$ = 73 ppm, Q^{*}_{feed} = 300 mL min^{-1}, and I = 38.4 W m^{-2} (measured within 280–400 nm: sunlight UV fraction); RH^{*}_{feed} = 30%, and T = 298 K; operation conditions reported in Table 2 (runs 3 and 7, respectively) (* Measured at 298 K and 1 bar); experimental data (points); mathematical modelling with RE-3 (lines).

parameters on the PCO of *n*-decane was assessed (e.g., photoreactor length L_R) within the operating condition studied, aiming unit geometric optimization and re-scaling. Fig. 7 shows the *n*-decane photodegradation fraction profiles, considering photoreactors of different lengths (L_R). It can be seen that, when the operating conditions of run 3 are employed (lowest incident irradiance, and intermediate feed flow rate and *n*-decane concentration), a 1.5-fold increase of the photoreactor length yields to a *n*-decane photodegradation enhancement of 85% (see Fig. 7a). Moreover, for a photoreactor 2× longer, complete *n*-decane photodegradation is attained (Fig. 7a). On the other hand, Fig. 7b predicts how *n*-decane photodegradation fraction is affected as a function of the photoreactor length when the highest incident irradiance and feed flow rate are employed (run 7). For a 1.5 times longer photoreactor than the experimentally employed, a 76% *n*-decane photodegradation enhancement is observed. If the reactor is twice the length (L_R = 0.32 m), only 1% of *n*-decane feed is predictively unreacted; complete *n*-decane photodegradation is attained when using a ~3 times longer photoreactor.

3.3. Reaction mechanism for the PCO of n-decane

The degradation mechanisms of alkanes and the corresponding formation of its by-products have been studied recently [61,64,66–69]. According to the previously cited authors it was found that ketones and aldehydes are the main intermediates of *n*-decane photochemical reaction. Minabe et al. [70] reported that gas-phase photooxidation of long organic chains over TiO_2 thin-films only produces CO_2 and H_2O. It was suggested that both reactants and intermediates were continuously adsorbed on the TiO_2 surface. Within this work, identification and quantification of the *n*-decane photocatalytic reaction by-products were monitored by GC/MSD (Supplementary Data: Table A.1), for the experimental conditions of run 1 (previously described in Table 2). The identified by-products (and their concentration) were: unreacted *n*-decane (4.32 ppm), *n*-hexane (0.035 ppm), *n*-heptane (0.028 ppm), *n*-octane (0.007 ppm), *n*-nonane (0.036 ppm), *n*-undecane (0.005 ppm), 4-methylnonane (0.006 ppm), 2,6-dimethyloctane (0.009 ppm), butanoic acid (0.022 ppm), propanoic acid (0.072 ppm), and butanal (0.016 ppm). Therefore and based on the nature of the identified compounds, a reaction mechanism under wet air (40%) is proposed and schematized in Scheme 1. According to Scheme 1, *n*-decane undergoes a cleavage into radicals – cracking – by a hydroxyl radical. Taking into consideration that alkyl radical stability increases along the series from methyl to primary, followed by secondary, and then by tertiary carbon, the energy required to create them decreases [71]. So, in the case of straight-chain alkanes, secondary carbons are oxidized by hydroxyl radical rather than primary ones. Nonetheless, from Scheme 1 and supported by literature [64,71–73], it is assumed the formation of both primary and secondary alkyl radicals. After homolytic cleavage of *n*-decane four paths can take place: (1) radical recombination generating new alkane hydrocarbons such as *n*-hexane, *n*-octane, or 2,6-dimethyloctane (Table 3); (2) hydrogen abstraction reactions leading to the formation of alkanes and alkenes; (3) reaction with adsorbed O_2 producing a highly reactive superoxide radicals; (4) oxidation by hydroxyl radicals forming alcohols.

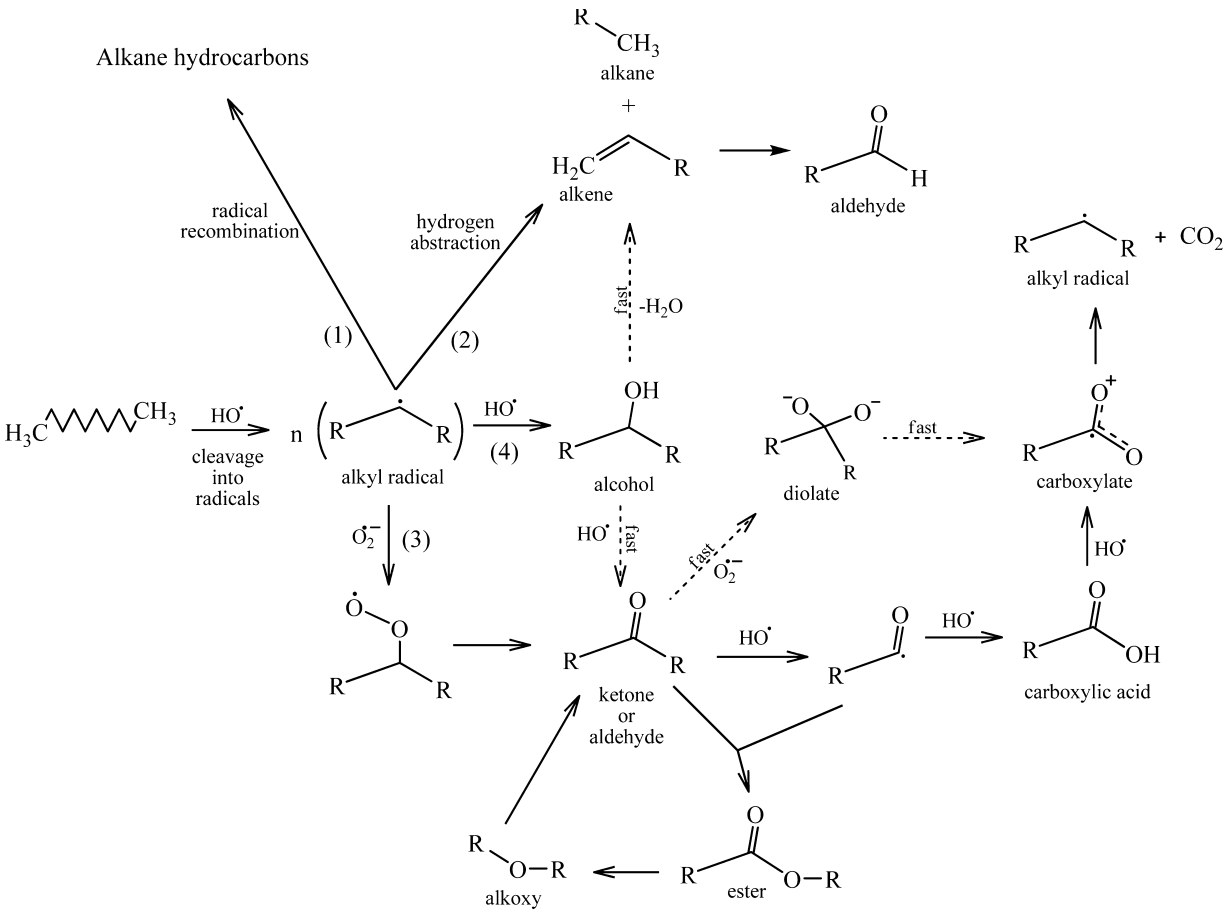

Scheme 1. Schematic representation of the reaction pathways proposed for the gas-phase degradation of *n*-decane under simulated solar irradiation (R: alkyl roots or hydrogen).

Several authors [24,64,67,73] reported the rapidly dehydration of alcohols into alkenes or oxidation into corresponding ketones or aldehydes (see Scheme 1, path 4); alkenes could be degraded into aldehydes as reported by Djeghri and Teichner [72] whereas aldehydes could suffer double oxidation by hydroxyl radicals into carboxylic acid [24,74,75] as it was detected the presence of propanoic and butanoic acid. An alternative approach was suggested by Kominami et al. [76] after observing the formation of an ester from the recombination of the aldehyde and its intermediate. Then, according to Augugliaro et al. [25] and Peral et al. [25], ester could be adsorbed on the TiO_2 surface where it would be dissociated into alkoxy and carboxylate radical. The alkoxy form an aldehyde and the carboxylate radical could produce alkyl radicals and carbon dioxide leading to alkanes after radical recombination or alkenes after hydrogen abstraction reaction. Carboxylate radical could also be formed by oxidation by hydroxyl radical of carboxylic acid which would lead to the formation of alkyl radicals and CO_2 in a process called decarboxylative dimerization. On the other hand, several authors [77–79] have proposed the reaction between ketones and adsorbed O_2, forming an unstable ketone diolate complex onto the TiO_2 surface. Consequently, the diolate complex would rapidly be dissociated into carboxylate which would lead to the formation of alkyl radicals and carbon dioxide. These radicals would be rapidly oxidized into alcohols and, then, aldehydes [80]. This approach may explain the absence of ketones and presence of butanal.

Considering that $C_{i,\,\text{C-dec}}$ refers to the carbon atoms concentration of compound *i* formed by *n*-decane photodegradation (all unreacted *n*-decane and its by-products produced), it can be defined as:

$$C_{i,\text{C-dec}} = \frac{C_i}{M_i} \cdot n(C) \cdot M(C) \tag{10}$$

where C_i (ppm) and M_i ($g\,mol^{-1}$) are the gas phase concentration and molecular weight of compound *i*, respectively, $n(C)$ is the number of carbon atoms of each component *i* molecule, and $M(C)$ ($g\,mol^{-1}$) is the molecular weight of a carbon atom. Thus, the mineralization efficiency (η_{min} in %) can be determined through Eq. (11).

$$\eta_{\text{min}}\ (\%) = \left[1 - \frac{\sum_i (C_{i,\text{C-dec}})_{\text{exit}}}{\sum_i (C_{i,\text{C-dec}})_{\text{feed}}}\right] \tag{11}$$

Thus, considering the carbon atoms concentration of each identified and quantified by-product resulting from the *n*-decane molecules photodegradation (experimental conditions reported in Table 1: run 1) more than 99% of the *n*-decane degraded (~94% of *n*-decane fed) was completely mineralized into CO_2 and H_2O. This result is in agreement to what Debono et al. [66] disclosed in their previous work: the total carbon atoms concentration of all by-products formed by *n*-decane photodegradation is lower than 5%.

4. Conclusion

The use of an annular lab-photoreactor under simulated solar irradiation has shown to be inefficient for the photochemical

reaction of gaseous *n*-decane and extremely effective on the photocatalytic process over a photo-TiO_2 paint. Under simulated solar irradiation, the gas-phase photocatalytic experiments showed that highest *n*-decane photodegradation (98%) was attained at the lowest Q_{feed} (75 $cm^3\ min^{-1}$) and $C_{dec,\ feed}$ (41 ppm), and highest RH_{feed} (40%) and *I* (38.4 $W\ m^{-2}$). Feeding the photoreactor with the double flow rate, the *n*-decane photodegradation decreases from 96 to 62% (runs 1 and 7). Alternatively, when the *n*-decane concentration on the feed stream is doubled, the remaining unreacted *n*-decane fed drops from 4 to 46% (runs 1 and 13). It was also observed that the water vapour content effect on the PCO of *n*-decane is more pronounced under lower irradiances, i.e., from ~71 to 56% (runs 3 and 18).

A phenomenological model, assuming a Langmuir-Hinshelwood mechanism (bimolecular competitive with two types of sites) was able to describe the *n*-decane photodegradation. It was observed proposed that both species compete for adsorption within different specific active sites (types 1 and 2) of the catalyst surface. Considering the type of by-products identified, a reaction mechanism for *n*-decane photodegradation under the conditions used was proposed.

For all reasons stated before and considering the well-known wide range of paint applications, the results reported seem quite promising for the treatment of indoor and outdoor air. Further research should focus in studying the role of interfering pollutants, as NO_2, and also the eventual production of acetaldehyde and formaldehyde as sub-products.

Acknowledgements

Financial support for this work was mainly provided by the FCT (Fundação para a Ciência e a Tecnologia) project PTDC/EQU-EQU/100554/2008. This work was also supported by project PEst-C/EQB/LA0020/2011, financed by FEDER through COMPETE – Programa Operacional Factores de Competitividade and by FCT. V.J.P. Vilar acknowledges financial support from Programme Ciência 2008 (FCT). R.A.R. Monteiro and J. Ângelo gratefully acknowledge FCT for their PhD Research Fellowships, SFRH/BD/69323/2010 and SFRH/BD/79974/2011, respectively. F.V.S. Lopes also gratefully acknowledge FCT for his Post-doc Research Fellowship, SFRH/BPD/73894/2010.

Appendix A. Supplementary data

Supplementary data associated with this article can be found, in the online version, at http://dx.doi.org/10.1016/j.apcatb.2013.09.031.

References

[1] C.H. Ao, S.C. Lee, C.L. Mak, L.Y. Chan, Appl. Catal. B: Environ. 42 (2003) 119.
[2] A.T. Hodgson, H. Destaillats, D.P. Sullivan, W.J. Fisk, Indoor Air 17 (2007) 305.
[3] J. Mo, Y. Zhang, Q. Xu, J.J. Lamson, R. Zhao, Atmos. Environ. 43 (2009) 2229.
[4] S.A. Grinshpun, A. Adhikari, T. Honda, K.Y. Kim, M. Toivola, K.S. Ramchander Rao, T. Reponen, Environ. Sci. Technol. 41 (2006) 606.
[5] M.A. Isbell, R.J. Stolzberg, L.K. Duffy, Sci. Total Environ. 345 (2005) 31.
[6] S. Wang, H.M. Ang, M.O. Tade, Environ. Int. 33 (2007) 694.
[7] J. Zhao, X. Yang, Build. Environ. 38 (2003) 645.
[8] C. Srinivasan, N. Somasundaram, Curr. Sci. 85 (2003) 1431.
[9] D.Y. Goswami, J. Sol. Energy Eng. 119 (1997) 107.
[10] M.R. Hoffmann, S.T. Martin, W. Choi, D.W. Bahnemann, Chem. Rev. 95 (1995) 69.
[11] D.S. Bhatkhande, V.G. Pangarkar, A.A.C.M. Beenackers, J. Chem. Technol. Biotechnol. 77 (2002) 102.
[12] C. McCullagh, J. Robertson, D. Bahnemann, P. Robertson, Res. Chem. Intermediat. 33 (2007) 359.
[13] D. Bahnemann, Sol. Energy 77 (2004) 445.
[14] R.W. Matthews, J. Chem. Soc. Faraday Trans. 1 (80) (1984) 457.
[15] J.M. Herrmann, Top. Catal. 34 (2005) 49.
[16] A.L. Linsebigler, G. Lu, J.T. Yates, Chem. Rev. 95 (1995) 735.
[17] M. Hernandez-Alonso, I. Tejedor-Tejedor, J. Coronado, J. Soria, M. Anderson, Thin Solid Films 502 (2006) 125.
[18] C. Guillard, J. Disdier, C. Monnet, J. Dussaud, S. Malato, J. Blanco, M.I. Maldonado, J.-M. Herrmann, Appl. Catal. B: Environ. 46 (2003) 319.
[19] M.L. Satuf, R.J. Brandi, A.E. Cassano, O.M. Alfano, Appl. Catal. B: Environ. 82 (2008) 37.
[20] E.M. Rossi, L. Pylkkänen, A.J. Koivisto, M. Vippola, K.A. Jensen, M. Miettinen, K. Sirola, H. Nykäsenoja, P. Karisola, T. Stjernvall, E. Vanhala, M. Kiilunen, P. Pasanen, M. Mäkinen, K. Hämeri, J. Joutsensaari, T. Tuomi, J. Jokiniemi, H. Wolff, K. Savolainen, S. Matikainen, H. Alenius, Toxicol. Sci. 113 (2010) 422.
[21] C.M. Sayes, R. Wahi, P.A. Kurian, Y. Liu, J.L. West, K.D. Ausman, D.B. Warheit, V.L. Colvin, Toxicol. Sci. 92 (2006) 174.
[22] R. Zhang, Y. Bai, B. Zhang, L. Chen, B. Yan, J. Hazard. Mater. 211/212 (2012) 404.
[23] J.V. Teixeira, S.M. Miranda, R.A.R. Monteiro, F.V.S. Lopes, J. Madureira, G.V. Silva, N. Pestana, E. Pinto, V.J.P. Vilar, R.A.R. Boaventura, Environ. Monit. Assess. 185 (2013) 59.
[24] J. Peral, D.F. Ollis, J. Catal. 136 (1992) 554.
[25] V. Augugliaro, S. Coluccia, V. Loddo, L. Marchese, G. Martra, L. Palmisano, M. Schiavello, Appl. Catal. B: Environ. 20 (1999) 15.
[26] E. Pelizzetti, C. Minero, Electrochim. Acta 38 (1993) 47.
[27] A. Furube, T. Asahi, H. Masuhara, H. Yamashita, M. Anpo, Chem. Phys. Lett. 336 (2001) 424.
[28] Y.V. Kolen'ko, K.A. Kovnir, A.I. Gavrilov, A.V. Garshev, P.E. Meskin, B.R. Churagulov, M. Bouchard, C. Colbeau-Justin, O.I. Lebedev, G. Van Tendeloo, M. Yoshimura, J. Phys. Chem. B 109 (2005) 20303.
[29] F. Benoit-Marquié, U. Wilkenhöner, V. Simon, A.M. Braun, E. Oliveros, M.-T. Maurette, J. Photochem. Photobiol. A 132 (2000) 225.
[30] L. Cermenati, P. Pichat, C. Guillard, A. Albini, J. Phys. Chem. B 101 (1997) 2650.
[31] A. Fujishima, K. Hashimoto, T. Watanabe, TiO_2 Photocatalysis: Fundamentals and Applications, BKC, Incorporated, Tokyo, 1999.
[32] E. Keidel, Furben Zeitung 34 (1929) 1242.
[33] C.F. Goodeve, J.A. Kitchener, Trans. Faraday Soc. 34 (1938) 570.
[34] H. Gerischer, in: H. Eyring, D. Henderson, W. Jost (Eds.), Physical Chemistry, An Advanced Treatise, Academic Press, New York, 1970, p. 463.
[35] V.A. Myamlin, Y.V. Pleskov, Electrochemistry of Semiconductors, Plenum Press, New York, 1967.
[36] S. Kato, F. Mashio, Abtr. Book Annu. Meet. Chem. Soc. Jpn. (1956) 223.
[37] A. Fujishima, K. Honda, Nature 238 (1972) 37.
[38] C.E. Bygott, J.E. Maltby, J.L. Stratton, R. McIntyre, International RILEM Symposium on Photocatalysis, Environment and Construction Materials, Florence, Italy, 8–9 October, 2007, p. 251.
[39] O. d'Hennezel, P. Pichat, D.F. Ollis, J. Photochem. Photobiol. A 118 (1998) 197.
[40] A. Bouzaza, A. Laplanche, J. Photochem. Photobiol. A 150 (2002) 207.
[41] C. Águia, J. Ângelo, L.M. Madeira, A. Mendes, Catal. Today 151 (2010) 77.
[42] J. Chen, C.-s. Poon, Build. Environ. 44 (2009) 1899.
[43] T. Salthammer, F. Fuhrmann, Environ. Sci. Technol. 41 (2007) 6573.
[44] T. Maggos, J.G. Bartzis, M. Liakou, C. Gobin, J. Hazard. Mater. 146 (2007) 668.
[45] J. Auvinen, L. Wirtanen, Atmos. Environ. 42 (2008) 4101.
[46] N.S. Allen, M. Edge, G. Sandoval, J. Verran, J. Stratton, J. Maltby, Photochem. Photobiol. 81 (2005) 279.
[47] L. Hochmannova, J. Vytrasova, Prog. Org. Coat. 67 (2010) 1.
[48] S. Laufs, G. Burgeth, W. Duttlinger, R. Kurtenbach, M. Maban, C. Thomas, P. Wiesen, J. Kleffmann, Atmos. Environ. 44 (2010) 2341.
[49] A. Costa, G.L. Chiarello, E. Selli, M. Guarino, J. Environ. Manage. 96 (2012) 86.
[50] V.M. Sousa, C.M. Manaia, A. Mendes, O.C. Nunes, J. Photochem. Photobiol. A 251 (2013) 148.
[51] C. Aguia, J. Angelo, L.M. Madeira, A. Mendes, J. Environ. Manage. 92 (2011) 1724.
[52] C. Águia, J. Ângelo, L.M. Madeira, A. Mendes, Polym. Degrad. Stabil. 96 (2011) 898.
[53] J. Kolarik, J. Toftum, Build. Environ. 57 (2012) 396.
[54] E. Uhde, T. Salthammer, Atmos. Environ. 41 (2007) 3111.
[55] O. Geiss, C. Cacho, J. Barrero-Moreno, D. Kotzias, Build. Environ. 48 (2012) 107.
[56] C. Chawengkijwanich, Y. Hayata, Int. J. Food Microbiol. 123 (2008) 288.
[57] M.A. Anderson, L.W. Miller, M.I. Tejedor-Anderson, Waveguide, United States Patent, Wisconsin Alumni Research Foundation, Madison, WI, US, 2001.
[58] F.V.S. Lopes, R.A.R. Monteiro, A.M.T. Silva, G.V. Silva, J.L. Faria, A.M. Mendes, V.J.P. Vilar, R.A.R. Boaventura, Chem. Eng. J. 204–206 (2012) 244.
[59] ISO 16000-6. Determination of volatile organic compounds in indoor and test chamber air by active sampling on Tenax TA sorbent, thermal desorption and gas chromatography using MS or MS/FID, 2004.
[60] F.V.S. Lopes, S.M. Miranda, R.A.R. Monteiro, S.D.S. Martins, A.M.T. Silva, J.L. Faria, R.A.R. Boaventura, V.J.P. Vilar, Appl. Catal. B: Environ 140/141 (2013) 444.
[61] A.K. Boulamanti, C.J. Philippopoulos, Atmos. Environ. 43 (2009) 3168.
[62] T.M. Twesme, D.T. Tompkins, M.A. Anderson, T.W. Root, Appl. Catal. B: Environ. 64 (2006) 153.
[63] P. Zhang, J. Liu, J. Photochem. Photobiol. A 167 (2004) 87.
[64] J. Shang, Y. Du, Z. Xu, Chemosphere 46 (2002) 93.
[65] S. Yamazaki, H. Tsukamoto, K. Araki, T. Tanimura, I. Tejedor-Tejedor, M.A. Anderson, Appl. Catal. B: Environ. 33 (2001) 109.
[66] O. Debono, F. Thévenet, P. Gravejat, V. Héquet, C. Raillard, L. Le Coq, N. Locoge, J. Photochem. Photobiol. A 258 (2013) 17.
[67] N. Djeghri, M. Formenti, F. Juillet, S.J. Teichner, Faraday Discuss. Chem. Soc. 58 (1974) 185.
[68] R. Nakamura, S. Sato, J. Phys. Chem. B 106 (2002) 5893.
[69] W. Balcerski, S.Y. Ryu, M.R. Hoffmann, Int. J. Photoenergy 2008 (2008), http://dx.doi.org/10.1155/2008/964721 (Article ID 964721).

[70] T. Minabe, D.A. Tryk, P. Sawunyama, Y. Kikuchi, K. Hashimoto, A. Fujishima, J. Photochem. Photobiol. A 137 (2000) 53.
[71] K.P.C. Vollhardt, N.E. Schore, Organic Chemistry: Structure and Function, 3rd ed., W.H. Freeman and Company, New York, 1999.
[72] N. Djeghri, S.J. Teichner, J. Catal. 62 (1980) 99.
[73] C. Hägglund, B. Kasemo, L. Österlund, J. Phys. Chem. B 109 (2005) 10886.
[74] E. Obuchi, T. Sakamoto, K. Nakano, F. Shiraishi, Chem. Eng. Sci. 54 (1999) 1525.
[75] X. Ye, D. Chen, J. Gossage, K. Li, J. Photochem. Photobiol. A 183 (2006) 35.
[76] H. Kominami, H. Sugahara, K. Hashimoto, Catal. Commun. 11 (2010) 426.
[77] C. Raillard, V. Héquet, P. Le Cloirec, J. Legrand, Water Sci. Technol. 53 (2006) 107.
[78] M.A. Henderson, Surf. Sci. 602 (2008) 3188.
[79] M.A. Henderson, J. Catal. 256 (2008) 287.
[80] E. Piera, J.A. Ayllón, X. Doménech, J. Peral, Catal. Today 76 (2002) 259.
[81] T. Valdés-Solís, M.J.G. Linders, F. Kapteijn, G. Marbán, A.B. Fuertes, Chem. Eng. Sci. 59 (2004) 2791.
[82] G.I. Taylor, Proc. R. Soc. Lond. A: Mater. 219 (1953) 186.
[83] A. Aris, Proc. R. Soc. Lond. A: Mater. 235 (1956) 67.
[84] D.M. Ruthven, Principal of Adsorption and Adsorption Processes, John Wiley & Sons, New York, 1984.
[85] B.E. Poling, J.M. Prausnitz, J.P. O'Connell, The Properties of Gases and Liquids, 5th ed., McGraw-Hill, New York, 2001.
[86] E.N. Fuller, K. Ensley, J.C. Giddings, J. Phys. Chem. 73 (1969) 3679.
[87] E.N. Fuller, J.C. Giddings, J. Chromatogr. Sci. 3 (1965) 222.
[88] E.N. Fuller, P.D. Schettler, J.C. Giddings, Ind. Eng. Chem. 58 (1966) 18.
[89] C.N. Satterfield, Mass Transfer in Heterogeneous Catalysis, MIT Press, Massachusetts Institute of Technology, Cambridge, MA, USA, 1970.
[90] G. Li Puma, I. Salvadó-Estivill, T.N. Obee, S.O. Hay, Sep. Purif. Technol. 67 (2009) 226.
[91] K.-H. Wang, H.-H. Tsai, Y.-H. Hsieh, Appl. Catal. B: Environ. 17 (1998) 313.
[92] T.N. Obee, R.T. Brown, Environ. Sci. Technol. 29 (1995) 1223.
[93] T.N. Obee, Environ. Sci. Technol. 30 (1996) 3578.
[94] T.N. Obee, S.O. Hay, Environ. Sci. Technol. 31 (1997) 2034.
[95] J. Peral, X. Domènech, D.F. Ollis, J. Chem. Technol. Biotechnol. 70 (1997) 117.